Internal structure visualization and lithographic use of periodic toroidal holes in liquid crystals

DONG KI YOON[1]*, M. C. CHOI[2,3]*, YUN HO KIM[1,4], MAHN WON KIM[2], OLEG D. LAVRENTOVICH[4] AND HEE-TAE JUNG[1]†

[1]Organic Opto-Electronic Materials Lab, Department of Chemical and Biomolecular Engineering (BK-21), Korea Advanced Institute of Science and Technology, Daejeon 305-701, Korea

[2]Department of Physics, Korea Advanced Institute of Science and Technology, Daejeon 305-701, Korea

[3]Materials Research Laboratory, University of California, Santa Barbara, California 93106, USA

[4]Liquid Crystal Institute and Chemical Physics Interdisciplinary Program, Kent State University, Kent, Ohio 44242, USA

*These authors contributed equally to this work

†e-mail: heetae@kaist.ac.kr

Published online: 14 October 2007; doi:10.1038/nmat2029

The formation of a large-area ordered structure by organic molecular soft building blocks is one of the most exciting interdisciplinary research areas in current materials science[1] and nanotechnology[2–4]. So far, several distinct organic building blocks—including colloids, block copolymers and surfactants—have been examined as potential materials for the creation of lithographic templates[1,5,6]. Here, we report that perfect ordered arrays of toric focal conic domains (TFCDs) covering large areas can be formed by semi-fluorinated smectic liquid crystals. Combined with controlled geometry, that is, a microchannel, our smectic liquid-crystal system exhibits a high density of TFCDs that are arranged with remarkably high regularity. Direct visualization of the internal structure of the TFCDs clearly verified that the smectic layers were aligned normal to the side walls and parallel to the top surface, and merge with the circular profile on the bottom wall surface. Moreover, we demonstrate a new concept: smectic liquid-crystal lithography. Grown in microchannels from a mixture of liquid-crystal molecules and fluorescent particles, TFCDs of the smectic liquid crystals acted as a template, trapping particles in an ordered array. Our findings pose new theoretical challenges and potentially enable lithographic applications based on smectic liquid-crystalline materials.

Toric focal conic domains (TFCDs) with a negative gaussian curvature, in which the bending smectic layers are ascribed to the presence of the defect pair formed by a circle and a straight line passing through the centre of the circle, have been well established in basic liquid-crystal research[7–10]. It is commonly accepted that the order and orientation of such domains are strongly affected by the molecular architecture and the controlled surface geometric properties. To implement our strategy, two rod-like molecules that are known to form smectic liquid crystals, one that is semi-fluorinated[11,12] **1** (4′-(5,5,6,6,7,7,8,8,9,9,10,10,11,-11,12,12,12-heptadecaflu-orododecyloxy)-biphenyl-4-carboxylic acid ethyl ester) and the other alkyl-terminated[13] **2** (4′-octyloxy-biphenyl-4-carboxylic acid ethyl ester), were prepared in Si microchannels (see the Methods section), as shown in Fig. 1. Materials **1** and **2** have several liquid-crystalline phases from smectic A (S_mA) to a crystal as the temperature decreases from that corresponding to the isotropic phase to room temperature.

In Fig. 2a, monodisperse circular patterns that are uniform in size are arranged in highly periodic patterns over a centimetre of channels. In addition, polarized optical microscopy (POM) images (Fig. 2b) of the film formed by **1** in the microchannels show that it has TFCDs, which is a typical characteristic of S_mA in the surface anisotropy condition[14]. Each TFCD produces a characteristic Maltese cross pattern, indicating that the projection of the director field onto the plane of the substrate is radial within the area bounded by the circular basis of the TFCD. Outside the circular base, the molecules are perpendicular to the bottom substrate (homeotropic alignment in between the TFCDs), and these regions appear dark under POM observation. TFCDs are arranged in periodically ordered arrays with an average centre to centre spacing of ∼2.5 μm. Each TFCD is associated with a depression of the S_mA free surface by a depth of ∼300 nm (see Fig. 2c and Supplementary Information, Fig. S8a). Depending on the width of the channel, we observe either linear arrays of TFCDs in narrow channels that are slightly wider than the diameter of a TFCD (Fig. 2a–c) or hexagonal arrays in the channels that are much wider than the diameter (Fig. 2d and Supplementary Information, Fig. S5). As the channel width varies, the quality of the hexagonal lattices also varies, apparently because the width of the channel should be commensurate with the lattice period to avoid distortions of the latter.

The cross-sectional electron microscope images reveal the internal structure of a TFCD. Figure 3a shows a fractured surface of a TFCD that cuts across the vertical axis of the domain, as illustrated in Fig. 3c. The S_mA layers are normal to the side walls and are curved towards the bottom plate at which they form concentric circles, as expected for TFCDs[7]. Some deviations of the layers from an ideal TFCD geometry can be caused by the roughness of the walls and by fracturing the sample. A section of the sample taken between

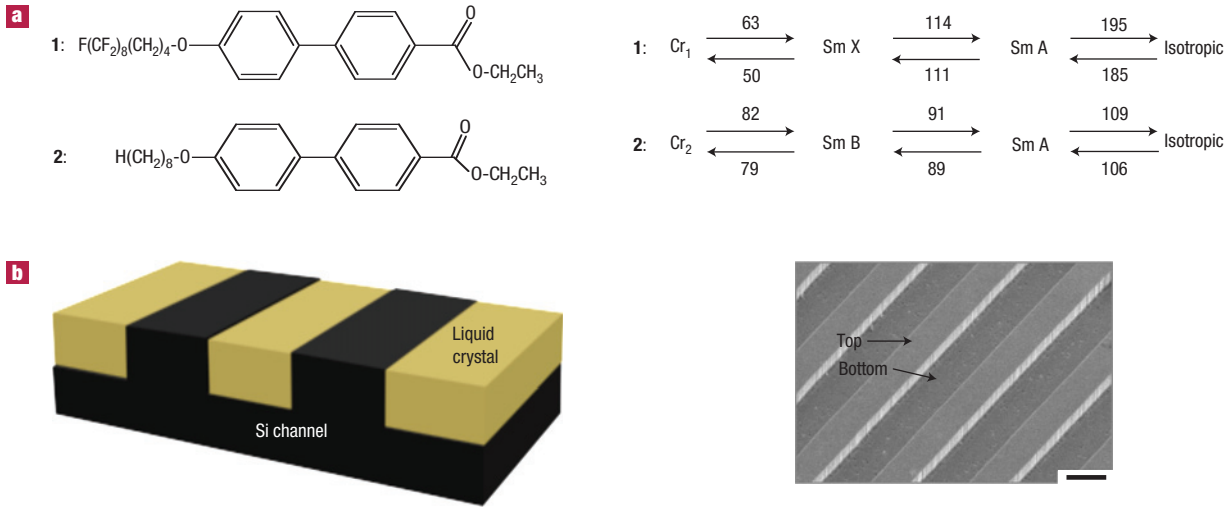

Figure 1 Liquid-crystal material and model of confined geometry. a, The structures, phases and transition temperatures of the rod-type liquid-crystal materials **1** and **2** (all temperatures are in degrees Celsius). **b**, Schematic representation of the space filling of compound **1** in the channels; the TFCDs are well aligned by the boundary condition. Bare Si channels are shown in the right panel (scale bar: 10 μm).

two neighbouring TFCDs, Fig. 3b,d, shows that the layers are flat and parallel to the bottom of the channel. This flat region between the TFCDs is dark under POM observation as the molecules are oriented along the optical axis. The curved layers within the TFCDs and flat layers outside the TFCDs match smoothly, as expected for TFCDs[7].

Our findings demonstrate that the two key parameters to achieve the long-range periodic lattices of liquid-crystal domains are (1) the molecular structure and (2) the surface properties of the confining geometry. The S_mA material **1** with fluorinated moieties consistently yields highly ordered hexagonal patterns of TFCDs in the channels, in contrast to other S_mA materials with alkyl-terminated liquid-crystal molecules that we have examined[15,16] thus far. The reason is not entirely clear, but it might be related to the fact that the molecule with the semi-fluorinated chain is more electronegative[17–19] than alkyl-terminated molecules[13,20,21], which causes the layered structure to be more stable[22] (it is known that by fluorinating molecular tails, nematic-forming materials are converted into smectic-forming materials[22]), and leads to a stronger tangential anchoring at the Teflon-AF (Dupont) walls of the channel.

The formation of a TFCD in a channel results from the balance of surface anchoring and elastic energies. As seen from the textures, the molecules prefer to be parallel to the walls and perpendicular to the free surface of the S_mA film. These boundary conditions can be satisfied only when the layers are bent, preferably with a minimum elastic energy cost. The latter is achieved by the construction of a TFCD, in which the defects are two singular lines: one is a circular line at the bottom and the other is a vertical straight line[7]. When a flat horizontal stack of S_mA layers is replaced with a TFCD, the total energy of the system decreases by the surface anchoring energy gain $\sim\pi a^2(\sigma_\parallel - \sigma_\perp) < 0$; here a is the TFCD radius and $\sigma_\parallel$ and $\sigma_\perp$ are the surface energy densities for molecules oriented parallel and perpendicular to the substrate, respectively, $\sigma_\parallel < \sigma_\perp$. The energy increase is accompanied by the elastic energy cost associated with the bent layers and two defect lines $\sim\alpha aK$, where K is the curvature elastic constant of S_mA and $\alpha \sim 1$–10 is a numerical factor[7]. The balance between two results in a minimum size of domain[23,24]

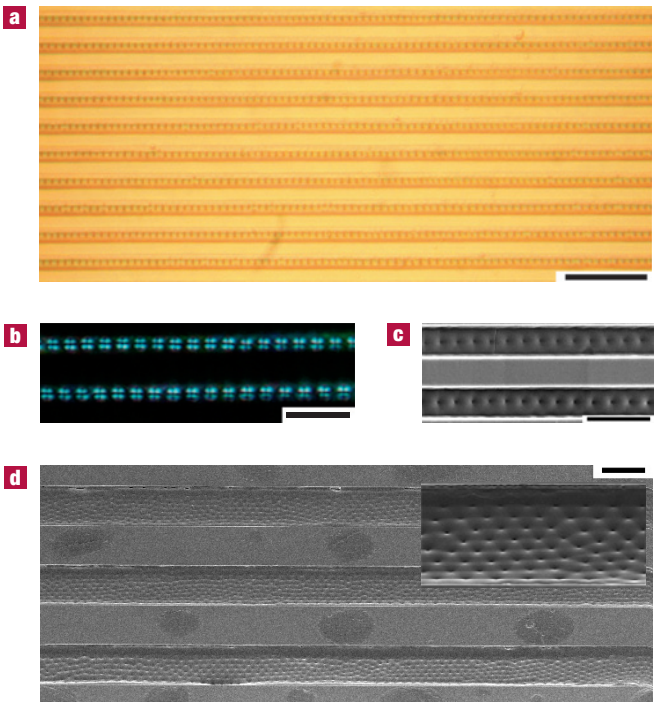

Figure 2 The dense population of TFCDs in the microchannels. a, Optical microscopy image of material **1** on Si microchannels of 5 μm width and depth. **b**,**c**, POM (**b**) and electron microscopy (**c**) images of the TFCDs in sample shown in **a**. **d**, Hexagonally ordered TFCDs throughout 50-μm-wide channels. Inset: Magnified image of one channel. Scale bars: **a**,**d**, 20 μm; **b**,**c**, 10 μm.

$a^* = \alpha K/2\pi(\sigma_\perp - \sigma_\parallel)$, which is of the order of 1–10 μm, for the typical estimates $K \sim 10$ pN and $\sigma_\perp - \sigma_\parallel \sim 10^{-5}$ J m^{-2}. The latter estimation can be modified so that we can take into account the extra surface tension term associated with the depression of the

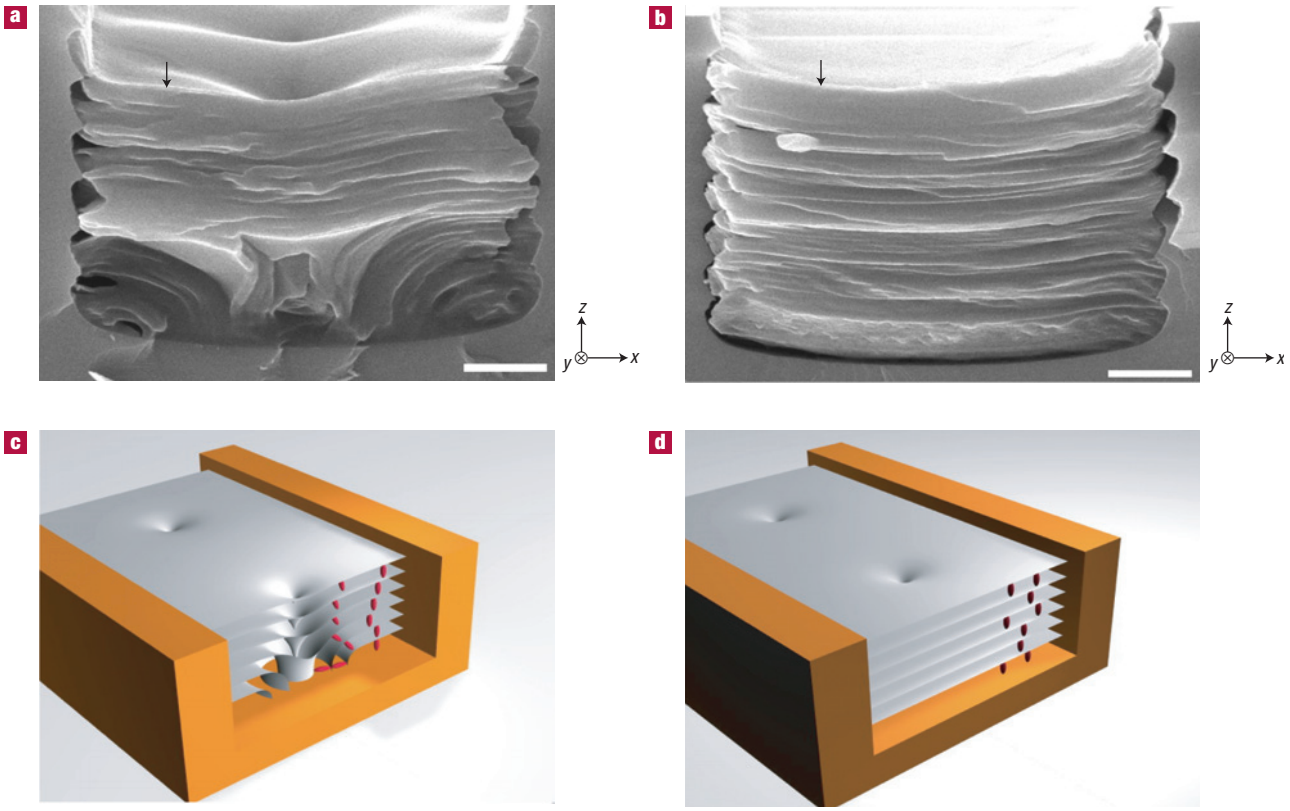

Figure 3 Direct visualization of the internal structure of the TFCDs. a,b, Direct visualization of TFCD (**a**) and non-toroidal homeotropic layers (**b**) in a microchannel. The arrows indicate the air–liquid-crystal interface. Scale bars: 1 μm. **c,d**, Schematic diagrams of **a** and **b**, respectively.

free surface[24], but the important feature to observe is that it is the tangential surface anchoring and rectangular confining geometry that drive the formation of TFCDs of size $a \geq a^*$. Note also that the domain size is restricted by the film thickness, that is, the depth of the channel (and, obviously, by the channel width when the latter is narrow): a too-large domain would be associated with a deep depression of the free surface and thus a large surface energy cost. The equilibrium size of a TFCD would thus depend on $K, \sigma_\perp - \sigma_\parallel$ and the surface tension of the free surface; the calculations associated with the previous estimates were carried out by Fournier and colleagues[24].

Let us now discuss why the TFCDs form a lattice. There are two important features that make arrays of TFCDs behave like a two-dimensional system of hard-core particles with purely repulsive interactions. First, the TFCDs can be embedded smoothly into the system of flat layers without losing the continuity of the S_mA layers, see ref. 7 and Fig. 3c,d. Second, the TFCDs are impenetrable to each other[8]; a penetration violates layer equidistance. Therefore, because each domain reduces the overall energy of the system, and because they cannot penetrate each other, we expect them to form a closely packed two-dimensional lattice, that is, a hexagonal structure, as observed in Fig. 2d. Of course, the separation between the TFCDs in the lattice can be influenced not only by the repulsive forces associated with impenetrability, but also by capillary forces associated with depressions of the free surface that are known to produce hexagonal patterns at the surface of a nematic liquid crystal[25].

We now demonstrate that TFCDs can be used as a template for a large-area particle array in the lithography technique. In Fig. 4a,b, the fluorescent silica particles were trapped in TFCDs, and arranged in a hexagonal structure. The y–z sectional confocal images of the smectic liquid-crystal film in the 100-μm-wide microchannel clearly show that the particles are predominantly localized in the middle of the 10-μm-thick film and at the vertical line defect of the toroidal domain.

To explain this phenomenon, we recall that the behaviour of a colloidal particle in the liquid-crystal environment is strongly dependent on the surface anchoring at the particle–liquid-crystal interface and the elasticity of the liquid-crystal host[26]. In particular, small particles tend to migrate towards linear defects such as disclinations thus reducing the overall energy of the system[27]. In our case, such a line is the vertical line defect. Another line defect is the circular base of the TFCD, but in our experiments, the particles are not observed there, despite the fact that further forces, such as gravity, might have favoured this location as opposed to the location in the bulk of the film. A plausible reason for the preferable particle location might be tangential surface anchoring of smectic molecules at the particles' surface. This type of anchoring is demonstrated in an independent experimental observation: large silica particles (diameter 4 μm) create two defect lines at the opposite poles that are compatible with the tangential anchoring, as demonstrated by Blanc and colleagues[28].

Let us consider the difference in the molecular structure at the core of the vertical and circular defects (Fig. 4c). Locally, the director $\hat{\mathbf{n}}$ around the circular defect is oriented normal to the defect core, forming a radial structure. At the vertical line defect, the situation is different: $\hat{\mathbf{n}}$ forms a cone with an angle at the apex $\chi = \arctan(a/z)$ (measured with respect to the z axis) that

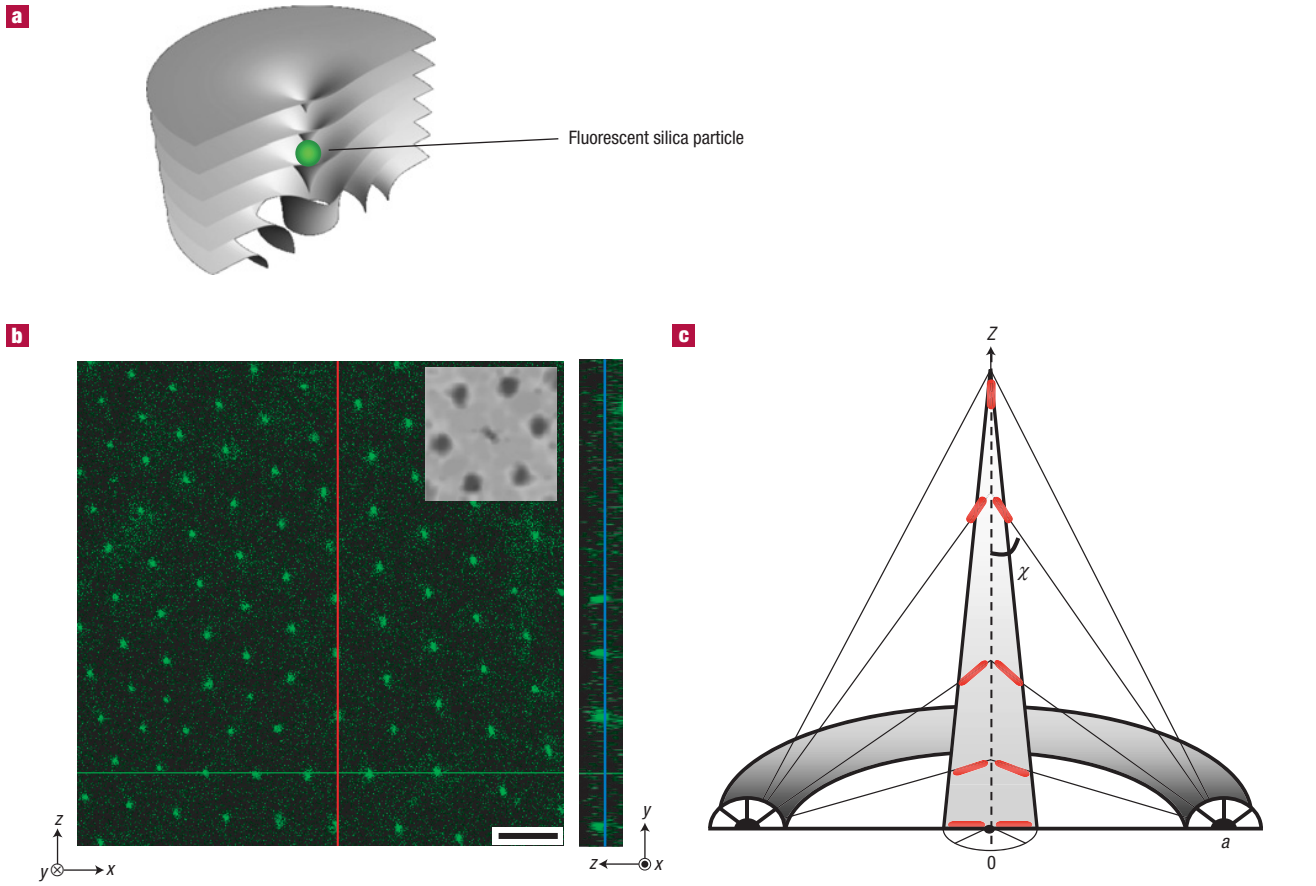

Figure 4 Trapped fluorescent silica particles in TFCDs. a, Schematic diagram of a silica particle trapped in the centre of a TFCD. **b**, Confocal microscopy image of 1 μm fluorescent silica particles trapped in a TFCD. The *y*–*z* sectional view along the red line is shown to the right. Inset: Two-dimensional fast Fourier transform (scale bar: 10 μm). **c**, Vertical cross-section of a TFCD showing the molecular structure near the defect core.

decreases from $\chi = \pi/2$ at the lower end of the defect, $z = 0$, to a smaller value as the z coordinate increases. The surface anchoring energy cost of placing the particle at different z locations along the axis can be estimated by integrating the standard Rapini–Papoular anchoring potential[5] over the spherical surface of the particle, $F_{\mathrm{anch}} = (\sigma_{\perp} - \sigma_{\parallel}) \oint [1 - (\hat{\mathbf{n}} \cdot \hat{\mathbf{v}})^2] \, \mathrm{d}s$, where $\hat{\mathbf{v}}$ is the normal to the particle's surface. We assume that the particle radius r is much smaller than the radius a of the TFCD, so that variations of χ at the particle's surface are neglected. A routine integration yields

$$F_{\mathrm{anch}} = \frac{4}{3}\pi r^2 (\sigma_{\perp} - \sigma_{\parallel}) \left(1 + \frac{1}{1+\delta^2}\right), \qquad (1)$$

where $\delta = z/a$; in other words, the larger z is, the smaller is the anchoring penalty for having the particle at the core of the defect. Note that the last formula is applicable for any location at the circular defect, in which case $\delta = 0$, and the anchoring energy assumes its maximum value. As for the vertical line defect, the vertically resolved force corresponding to the potential (1) and pushing the particle upwards, $f_{\mathrm{anch}} = -\partial F_{\mathrm{anch}}/\partial z = (8/3)\pi r^2 (\delta/a(1+\delta^2)^2)(\sigma_{\perp} - \sigma_{\parallel})$, is significant: for the typical[7] $(\sigma_{\perp} - \sigma_{\parallel}) \approx 10^{-5}\,\mathrm{J\,m^{-2}}$, $r = 0.5\,\mu\mathrm{m}$, $a = 2\,\mu\mathrm{m}$ and $\delta \sim 1$, we find $f_{\mathrm{anch}} \approx 10\,\mathrm{pN}$, much larger than the gravity force $f_g = (4/3)\pi r^3 \rho g \sim 0.01\,\mathrm{pN}$ (here $\rho \sim 10^3\,\mathrm{kg\,m^{-3}}$ is the difference in the densities of a silica particle and a liquid crystal, and $g = 9.8\,\mathrm{m\,s^{-2}}$ is the standard gravity). The presented analysis is only qualitative, but it outlines a possible mechanism for the 'lifting' force that keeps the particle above the bottom of the microchannel, at the core of the vertical defect; a complete consideration would require a detailed analysis of the elastic forces of bending and compressing the layers, interaction with the surfaces of the sample and so on.

The smectic liquid-crystal lithography technique presented here has notable features: a well-ordered structure of TFCDs was generated by semi-fluorinated smectic liquid crystals in a controlled geometry on the micrometre scale. Our system introduces a new concept for lithography templates using organic building blocks, whereby an ordered array of artificially made defects (TFCDs) is introduced into a confined system, whereas previous studies on self-assembling materials have been geared towards defect-free systems of cylindrical and spherical phases. In addition, the ordered array of TFCDs forms rapidly owing to the reversible and non-covalent interactions between the liquid-crystal molecules, and can be easily generated by controlling surface anchoring, which is a very simple and cost-effective mechanism that is well suited to mass production. It was verified that the ordered arrays of TFCDs can be used as templates by assessing particle trapping. This soft building block system poses new theoretical challenges and potentially enables new optoelectronic applications. In particular, the demonstrated technique to control not only the size of the domains but also their ordering is important for its potential technological applications.

METHODS

FABRICATION OF CONTROLLED SURFACE GEOMETRY

Microchannels were fabricated on (100)Si wafers using photolithography and reactive ion etching techniques[29]. The microchannels had a square cross-section and were 5 μm deep, 3 to 100 μm wide and 10 mm long. To control the surface polarity, the channels were chemically cleaned by ultrasonication in a mixture of dimethylformamide (DMF) and methanol to remove organic/inorganic impurities, followed by rinsing several times with deionized water. To produce a perfect tangential surface anchoring of the S_mA (material **1**) at the bottom substrate, a fluorinated polymer (Teflon-AF, Dupont) was spin-coated from a solution in organic fluorinated solvent (Fluorinert FC-77, 3M); the alignment material was not treated further after drying.

PREPARING MICROSCOPY SAMPLES

Microchannels were cleaned using a mixture of DMF and methanol to remove organic/inorganic impurities, followed by rinsing several times with deionized water. The crystalline powder of the S_mA material was placed in the channel and then heated to beyond the temperature (195 °C) corresponding to the isotropic phase with a Mettler FP82 and FP90 thermo-system hot stage to fill the microchannel by capillary action. The amount of dry powder was controlled to fill the channels properly. The sample was then cooled down to the S_mA phase (from 195 to 114 °C) at a rate of 10 °C min^{-1}. (The transition temperatures were examined using a 2010 thermal analyser (Dupont) under N_2 flow at a scanning rate of 5 °C min^{-1}.) The textures of the liquid crystals at different phases were monitored *in situ* under a polarized light microscope (DMLB, Leica), equipped with a hot stage (FP82 and FP90, Mettler). To prepare electron micrography samples, liquid crystals were coated with a 10 nm layer of Pt to improve electron sensitivity and to protect the sample from beam damage. Images of the ordered liquid-crystal domains were obtained using a scanning electron microscope (Sirion FE-SEM, FEI). The trapped silica particles containing N,N′-bis(2,5,-di-*tert*-butylphenyl)-3,4,9,10-phenylenedicarboxyimide; Aldrich) dye were probed by a fluorescence confocal microscope (LSM510-META NLO, Carl Zeiss). The excitation and emission wavelengths were 488 nm and 510–550 nm, respectively. 10 μl of fluorescent silica particles (purchased from Corpuscular) with a mean diameter of 1 μm at a concentration of 1 wt% in water were mixed with 500 μl of liquid-crystal solution at a concentration of 1 wt% in DMF solvent at 70 °C for thorough mixing, after which the solvent was removed by Ar purging for about 5 h. The resulting sample was heated to the isotropic phase on a substrate and cooled at 10 °C min^{-1} to the liquid-crystal phase.

Received 19 March 2007; accepted 28 August 2007; published 14 October 2007.

References

1. Cao, G. *Nanostructures and Nanomaterials: Synthesis, Properties & Applications* (Imperial College Press, New York, 2004).
2. Whitesides, G. M. & Grzybowski, B. Self-assembly at all scales. *Science* **295**, 2418–2421 (2002).
3. Stenzel, M. H., Barner-Kowollik, C. & Davis, J. P. Formation of honeycomb-structured, porous films via breath figures with different polymer architectures. *J. Polym. Sci. A* **44**, 2363–2375 (2006).
4. Barth, J. V., Costantini, G. & Kern, K. Engineering atomic and molecular nanostructures at surfaces. *Nature* **437**, 671–679 (2005).
5. Jones, R. A. *Soft Condensed Matter* (Oxford Univ. Press, New York, 2002).
6. Cheng, J. Y., Mayes, A. M. & Ross, C. A. Nanostructure engineering by templated self-assembly of block copolymers. *Nature Mater.* **3**, 823–828 (2004).
7. Kleman, M. & Lavrentovich, O. D. *Soft Matter Physics* (Springer, New York, 2003).
8. Li, Z. & Lavrentovich, O. D. Surface anchoring and growth pattern of the field-driven first-order transition in a smectic-A liquid crystal. *Phys. Rev. Lett.* **73**, 280–284 (1994).
9. Choi, M. C. *et al.* Ordered patterns of liquid crystal toroidal defects by microchannel confinement. *Proc. Natl Acad. Sci. USA* **101**, 17340–17344 (2004).
10. Dierking, I. *Textures of Liquid Crystals* (Wiley-VCH, Weinheim, 2003).
11. Johansson, G., Percec, V., Ungar, G. & Zhou, J. P. Fluorophobic effect in the self-assembly of polymers and model compounds containing tapered groups into supramolecular columns. *Macrocmolecules* **29**, 646–660 (1996).
12. Johansson, G., Percec, V., Ungar, G. & Smith, K. Fluorophobic effect generates a systematic approach to the synthesis of the simplest class of rodlike liquid crystals containing a single benzene unit. *Chem. Mater.* **9**, 164–175 (1997).
13. Gray, G. W. & Goodby, J. W. Some effects of small changes in molecular framework on the incidence of smectic C and other smectic liquid crystal phases in esters. *Mol. Cryst. Liq. Cryst.* **37**, 157 (1976).
14. de Gennes, P.-G. & Prost, J. *The Physics of Liquid Crystals* (Clarendon, Oxford, 1993).
15. Lee, E. H. *et al.* Alignment of perfluorinated supramolecular columns on the surfaces of various self-assembled monolayers. *Macromolecules* **38**, 5152–5157 (2005).
16. Yoon, D. K. *et al.* Large-area, highly aligned cylindrical semi-fluorinated supramolecular dendrimers using magnetic fields. *Adv. Mater.* **18**, 509–513 (2006).
17. Percec, V. *et al.* Self-organization of supramolecular helical dendrimers into complex electronic materials. *Nature* **419**, 384–387 (2002).
18. Tomalia, D. A. Supramolecular chemistry—fluorine makes a difference. *Nature Mater.* **2**, 711–712 (2003).
19. Percec, V. *et al.* Self-assembly of amphiphilic dendritic dipeptides into helical pores. *Nature* **430**, 764–768 (2004).
20. Jung, H.-T. *et al.* Elastic properties of hexagonal columnar mesophase self-organized from amphiphilic supramolecular columns. *Appl. Phys. Lett.* **80**, 395–397 (2002).
21. Jung, H.-T., Lee, S.-Y., Kaler, E. W., Coldren, B. & Zasadzinski, J. A. Gaussian curvature and the equilibrium among bilayer cylinders, spheres, and discs. *Proc. Natl Acad. Sci. USA* **99**, 15318–15322 (2002).
22. Pivovarova, N. S., Boldescul, I. E., Lavrentovich, O. D., Shelyazhenko, S. V. & Fialkov, Y. A. Mesomorphism of MBBA fluorinated derivatives. *Kristallografiya* **33**, 1460–1463 (1988).
23. Lavrentovich, O. D. Hierarchy of defect structures in space filling by flexible smectic-A layers. *Sov. Phys. JETP* **64**, 984 (1986).
24. Fournier, J. B., Dozov, I. & Durand, G. Surface frustration and texture instability in smectic-A liquid crystals. *Phys. Rev. A* **41**, 2252–2255 (1990).
25. Smalyukh, I. I. *et al.* Ordered droplet structures at the liquid crystal surface and elastic-capillary colloidal interactions. *Phys. Rev. Lett.* **93**, 117801–117804 (2004).
26. Poulin, P., Stark, H., Lubensky, T. C. & Weitz, D. A. Novel colloidal interactions in anisotropic fluids. *Science* **275**, 1770–1773 (1997).
27. Voloschenko, D., Pishnyak, O. P., Shiyanovskii, S. V. & Lavrentovich, O. D. Effect of director distortions on morphologies of phase separation in liquid crystals. *Phys. Rev. E* **65**, 060701–060704 (2002).
28. Blanc, C. & Kleman, M. The confinement of smectics with a strong anchoring. *Eur. Phys. J. E* **4**, 241–251 (2001).
29. Madou, M. J. *Fundamentals of Microfabrication* (CRC Press, LLC, 2002).

Acknowledgements

This work was supported by the National Research Laboratory Program of the Korea Science and Engineering Foundation (KOSEF), the Basic Research Program (R01-2005-000-10456-0), the KRF (2005-908-D00018), the Korea Health 21 R&D Project of MOHW and the CUPS-ERC program. X-ray experiments were carried out at PLS were supported in part by MOST and POSCO. M.C.C. received partial support from the Korean Research Foundation Grant KRF-2005-2214-C00202. O.D.L. acknowledges the support of a NSF DMR 0504516 grant.

Correspondence and requests for materials should be addressed to H.-T.J.

Supplementary Information accompanies this paper on www.nature.com/naturematerials.